Abstract

Seismic safety evaluation of earth works on liquefiable ground currently uses Δu-method or seismic coefficient method to calculate the factor of safety in Japan. Recently, coupled effective stress dynamic analysis is gradually used to calculate the residual displacement induced by the earthquake including the possible liquefaction. This paper proposes to use seepage analysis, fully coupled effective stress dynamic analysis, and shear strength reduction technique to calculate the residual displacement and the factor of safety of embankments. We analyzed the Lower and Upper San Fernando Dam using the proposed approaches. The major slide for the Lower San Fernando Dam and the residual displacement for the Upper San Fernando dam were re-produced well.

Keywords: embankment, liquefaction, slope stability, finite element method, limit equilibrium method, seismic design.

1 Introduction

Seismic coefficient method is conventionally used to calculate the factor of safety of embankment stability assuming a circle slip surface; for liquefiable embankments, the Δu-method is used to estimate the seismic stability of embankments in Japan. In the Δu-method, empirical analysis is used to estimate excess pore water pressure induced by earthquake, and conventional stability analysis is used to calculate the factor of safety. Because of potential limitations in the seismic coefficient method and the called Δu-method, dynamic analysis procedure has been proposed to evaluate behaviours of embankments under strong earthquakes [1, 2].

Dynamic analysis procedure is mainly used to evaluate the residual displacement of embankments under strong earthquakes, and the seismic stability of embankments is mainly evaluated based on the calculated residual displacement. However, for liquefiable embankments, most sliding failures occurred after main shaking of

earthquake [2]. The Lower San Fernando Dam is a famous example [3]. It is necessary for the liquefiable embankments to calculate the stability after the earthquake considering the excess pore water pressure induced by the main shaking of earthquake.

This paper proposes to use finite element approaches to evaluate the seismic safety of embankments under strong earthquake; in details, we use finite element seepage analysis to calculate the pore water pressure before earthquake, use fully coupled dynamic elastoplastic finite element approach to calculate the residual displacement and excess pore water pressure induced by strong earthquake, and use static elastoplastic finite element method with shear strength reduction technique to evaluate the safety of embankments after strong earthquake considering the pore water pressure calculated by finite element seepage analysis and excess pore water pressure calculated by fully coupled dynamic elastoplastic finite element approach. The factor of safety of embankments of the finite element approaches is compared with those of conventional Δu-method or seismic coefficient method.

2 Analysis Procedure

2.1 Analysis Procedure

The analysis procedure involves a series of steps, and it is basically similar to that advised by Seed et al. [1, 2].

(1) Select the cross-section of the embankment to be analyzed, input motion, and water level for seismic design.
(2) Discrete the selected cross-section using finite element mesh.
(3) Identify the parameters necessary for the analyses, included hydraulic properties for seepage analysis, parameters of selected constitutive models used in static and dynamic finite element analyses.
(4) Conduct finite element seepage analysis to evaluate the distribution of pore water pressure under the water level selected in step (1) before the earthquake.
(5) Calculate the stresses existing in the embankment before the earthquake considering the pore water pressure evaluated in step (4). We use total stress analysis to evaluate the initial stress in the embankment, considering the pore water pressure as equivalent nodal loads, and using an elastic-perfectly plastic constitutive relationship defined by a yield surface of Mohr-Coulomb type and a plastic potential of Drucker-Prager type.
(6) Conduct fully coupled effective stress dynamic finite element analysis to evaluate the residual displacement and excess pore water pressure induced by the input motion selected in step (1). We use the Pastor-Zienkiewicz model for all types of soils.
(7) Evaluate the seismic stability of the embankment using the sum of the pore water pressure before the earthquake and the excess pore water pressure induced by the earthquake. We use the elasto-perfectly plastic finite element method in conjunction with shear strength reduction technique and limit equilibrium method to evaluate the seismic stability.

2.2 Analysis Methods

We use VisualFEA+VGFlow [9] a finite element seepage analysis software to evaluate the pore water pressure before the earthquake, UWLC [10] a fully coupled effective stress dynamic finite element program to calculate the residual displacement and excess pore water pressure in the embankment induced by the earthquake, and GeoFEAS [11] a static elastoplastic finite element program to calculate the initial stress in the embankment and to estimate the stability of the embankment.

2.2.1 Fully Coupled Dynamic Finite Element Analysis

A basic fully coupled effective-stress procedure is formulated based on the balance of momentum and conservation of masses. For a saturated soil subjected to cyclic loading, the dynamic equations of motion can be written following Biot. After the spatial finite element discretization of the displacement and excess pore water pressure, the governing equations for the solid-fluid mixture and fluid phase at any time can be written as:

$$\mathbf{M}\ddot{\mathbf{u}} + \mathbf{K}\mathbf{u} - \mathbf{Q}\mathbf{p} = \mathbf{f}^{u} \tag{1}$$

$$\mathbf{Q}^{T}\dot{\mathbf{u}} + \mathbf{H}\mathbf{p} + \mathbf{S}\dot{\mathbf{p}} = \mathbf{f}^{p} \tag{2}$$

where $\mathbf{M}$ is the global mass matrix, $\mathbf{K}$ is the global stiffness matrix, $\mathbf{Q}$ is the coupling matrix, $\mathbf{H}$ is the permeability matrix, $\mathbf{S}$ is the compressibility matrix, $\mathbf{u}$ is the displacement vector, $\mathbf{p}$ is the excess pore water pressure vector , $\mathbf{f}^{u}$ is the force vector for the solid-fluid mixture, and $\mathbf{f}^{p}$ is the force vector for the fluid phase.

To complete the numerical solution, it is necessary to integrate the ordinary differential Equations (1) and (2) in time by one of the many available schemes. The unconditionally stable generalized Newmark method is used in UWLC [10]. In this method, the acceleration, velocity, and displacement at time station t_{n+1} are linked with those at time station t_n:

$$\ddot{\mathbf{u}}_{n+1} = \ddot{\mathbf{u}}_{n} + \Delta\ddot{\mathbf{u}}_{n} \tag{3}$$

$$\dot{\mathbf{u}}_{n+1} = \dot{\mathbf{u}}_{n} + (1+\theta_1)\Delta\ddot{\mathbf{u}}_{n}\Delta t \tag{4}$$

$$\mathbf{u}_{n+1} = \mathbf{u}_{n} + \Delta\dot{\mathbf{u}}_{n}\Delta t + \frac{1}{2}(1+\theta_2)\Delta\ddot{\mathbf{u}}_{n}\Delta t^{2} \tag{5}$$

The rate of the excess pore water pressure change and the excess pore water pressure at time station t_{n+1} are given by:

$$\dot{\mathbf{p}}_{n+1} = \dot{\mathbf{p}}_{n} + \Delta\dot{\mathbf{p}}_{n} \tag{6}$$

$$\mathbf{p}_{n+1} = \mathbf{p}_n + (1+\theta)\Delta\dot{\mathbf{p}}_n \Delta t \tag{7}$$

In Equations (3)-(7), $\Delta\ddot{\mathbf{u}}_n$ and $\Delta\dot{\mathbf{p}}_n$ are as yet unknown quantities. The parameters θ_1, θ_2, and θ are usually chosen as $\theta_1 \geq \theta_2 \geq 1/2$ and $\theta \geq 1/2$ for unconditionally stability of the scheme. Substituting Equations (3)-(7) into Equations (1)-(2), we can obtain:

$$\begin{bmatrix} \mathbf{M} + \frac{1}{2}\theta_2 \Delta t^2 \mathbf{K} & -\theta\Delta t\mathbf{Q} \\ -\theta\Delta t\mathbf{Q}^T & -\left(\theta\Delta t\mathbf{H} + \frac{\theta}{\theta_1}\mathbf{S}\right) \end{bmatrix} \begin{Bmatrix} \Delta\ddot{\mathbf{u}}_n \\ \Delta\dot{\mathbf{p}}_n \end{Bmatrix} = \begin{Bmatrix} \boldsymbol{\psi}^u_{n+1} \\ \boldsymbol{\psi}^p_{n+1} \end{Bmatrix} \tag{8}$$

The residual on the right hand of Equation (8) is given by:

$$\boldsymbol{\psi}^u_{n+1} = \mathbf{f}^u_{n+1} - \mathbf{M}_{n+1}\ddot{\mathbf{u}}_{n+1} - \int_\Omega \mathbf{B}^T_{n+1}\boldsymbol{\sigma}'_{n+1} d\Omega + \mathbf{Q}_{n+1}\mathbf{p}_{n+1} \tag{9}$$

$$\boldsymbol{\psi}^p_{n+1} = -\frac{\theta}{\theta_1}\left(\mathbf{f}^p_{n+1} - \mathbf{Q}^T_{n+1}\dot{\mathbf{u}}_{n+1} - \mathbf{H}_{n+1}\mathbf{p}_{n+1} - \mathbf{S}_{n+1}\dot{\mathbf{p}}_{n+1}\right) \tag{10}$$

Equation (8) is nonlinear, and it is solved by initial stiffness method in UWLC [10].

Soil behaviour under earthquake loading is complex. It is essential that the constitutive relationship used in the fully coupled effective-stress dynamic finite element analysis should be able to capture important features of soil response under cyclic loading such as dilatancy, hysteresis loops, and permanent deformation. UWLC uses the generalized plasticity model [6, 7] for sand.

2.2.2 Static Elastoplastic Analysis

We use GeoFEAS to calculate the initial stresses in the embankment before the earthquake, and to evaluate the slope stability of the embankment. Though GeoFEAS is a static total-stress finite element code, it takes the pore water pressure as an external force. Consequently, it can be used to estimate the influence of the excess pore water pressure induced by the earthquake on the shear strength and then on the stability of the embankment.

The initial stresses in the embankment before the earthquake were calculated taking the self weight of soils and the pore water pressure as the external forces. The pore water pressure was calculated using the steady seepage analysis. The method to calculate the equivalent nodal forces of the pore water pressure is shown in section 2.3 of this paper. The soils were considered as an elastic-perfectly plastic material, defined by a yield function of Mohr-Coulomb type, and a plastic potential of Drucker-Prager type.

The stability of the embankment was also estimated using a static elastoplastic finite element analysis in conjunction with the shear strength reduction technique. In

the elastoplastic finite element method in conjunction with the shear strength reduction technique, the safety factor emerges naturally from the analysis without the user having to commit to any particular form of the slip surface in advance [12]. The excess pore water pressure induced by the earthquake was considered as an external force.

2.3 Pore Water Pressure

To calculate the equivalent nodal forces induced by the pore water pressure, first, we calculate the body forces (buoyancy and seepage forces) at the Gaussian integration points using the shape function and nodal pore water pressure. The body forces in x- and y-directions are given by Equations (1) and (2) respectively:

$$\gamma_w i_x = -\gamma_w \frac{\partial h}{\partial x} = -\frac{\partial p}{\partial x} = -\sum_{i=1}^{n} \frac{\partial N_i}{\partial x} p_i \tag{11}$$

$$\gamma_w i_y + \gamma_w = -\gamma_w \frac{\partial h}{\partial y} + \gamma_w = -\frac{\partial p}{\partial y} = -\sum_{i=1}^{n} \frac{\partial N_i}{\partial y} p_i \tag{12}$$

where i_x and i_y are the hydraulic gradient in the x- and y-directions respectively, h is the hydraulic head, p is the pore water pressure, γ_w is the unit weight of water, N_i is the shape function, p_i is the nodal pore water pressure, and n is the number of the nodes of one element.

Second, the equivalent nodal forces of the pore water pressure are given by:

$$\mathbf{f}_x^p = -\int_\Omega \mathbf{N}^T \frac{\partial p}{\partial x} d\Omega \tag{13}$$

$$\mathbf{f}_y^p = -\int_\Omega \mathbf{N}^T \frac{\partial p}{\partial y} d\Omega \tag{14}$$

If Equations (11)-(14) are used to calculate the equivalent nodal forces of the pore water pressure at nodes, it is not necessary to consider the water pressure on the boundary as an external distributed load.

When limit equilibrium methods are used to evaluate the seismic stability considering the pore water pressure including the pore water pressure before the earthquake and the excess pore water pressure induced by the earthquake, we have to calculate the pore water pressure on the slip surface using the pore water pressure at the nodes of the finite element mesh. Assuming an arbitrary point A located on the slip surface, we can calculate the pore water pressure at the point A using the following steps:

(1) Pick up the element inside that the point A locates using the coordinates of the point A (x_A, y_A).

(2) Calculate the local coordinates (ξ_A, η_A) of the point A. We can directly calculate the local coordinates for 4-node isoparametric element; however, iteration is necessary for 8-node isoparametric [5].
(3) Calculate the pore water pressure at the point A using the shape function and nodal pore water pressure using Equation (15):

$$p_A = \sum_{i=1}^{n} N_i(\xi_A, \eta_A) p_i \tag{15}$$

3 The Lower and Upper San Fernando Dams

The Lower and Upper San Fernando Dams were located northwest of Los Angles, and they were within about three kilometres of each other. Both of the dams were constructed in the period 1915-1925. However, the stability of the Lower Dam had been evaluated in 1966, and it had been considered to be adequately resistant to earthquake effects.

The Lower San Fernando Dam was essentially a hydraulic fill embankment capped by a potpourri of wagon-dumped and rolled fills. The embankment was about 43.7m high at its maximum section and was founded on 9.5m recent alluvium deposits consisting of stiff clay with lenses of sand and gravel. A typical cross-section of the Lower Dam is shown in Figure 1.

The Upper San Fernando Dam was constructed using a semi-hydraulic fill technique. The embankment was about 24.4m high and was constructed on 15.2 m recent alluvial deposits consisting of stiff clay and clayey gravel. A typical cross-section of the Upper Dam is shown in Figure 2.

During the 1971 San Fernando Earthquake, the Lower San Fernando Dam experienced a major slide in the upstream shell, as shown in Figure 3. In comparison, the Upper San Fernando Dam moved 1.5-2.1m downstream as the results of the shaking; the movement was significant, but limited, as shown in Figure 4.

A detailed description of the construction and history of the Lower and Upper San Fernando Dams and their seismic behaviour during the 1971 San Fernando Earthquake can be found in Reference [3].

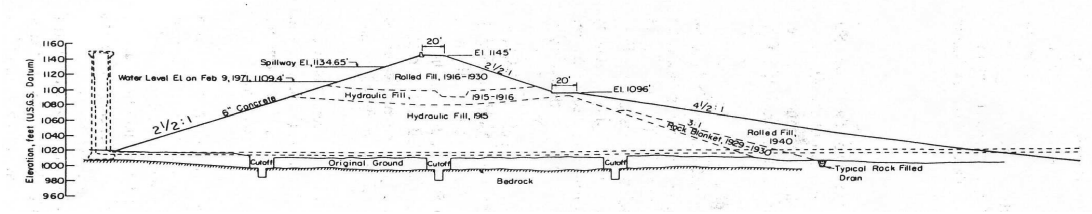

Figure 1: Typical cross-section of the lower San Fernando Dam (after Reference [3]).

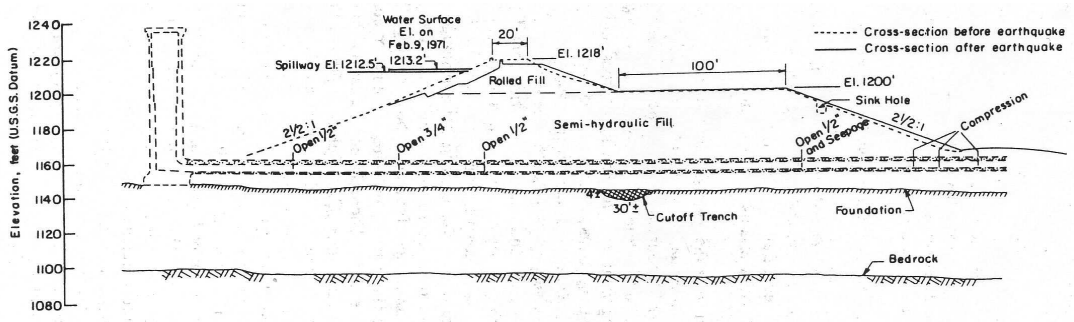

Figure 2: Typical cross-section of the upper San Fernando Dam (after Reference [3]).

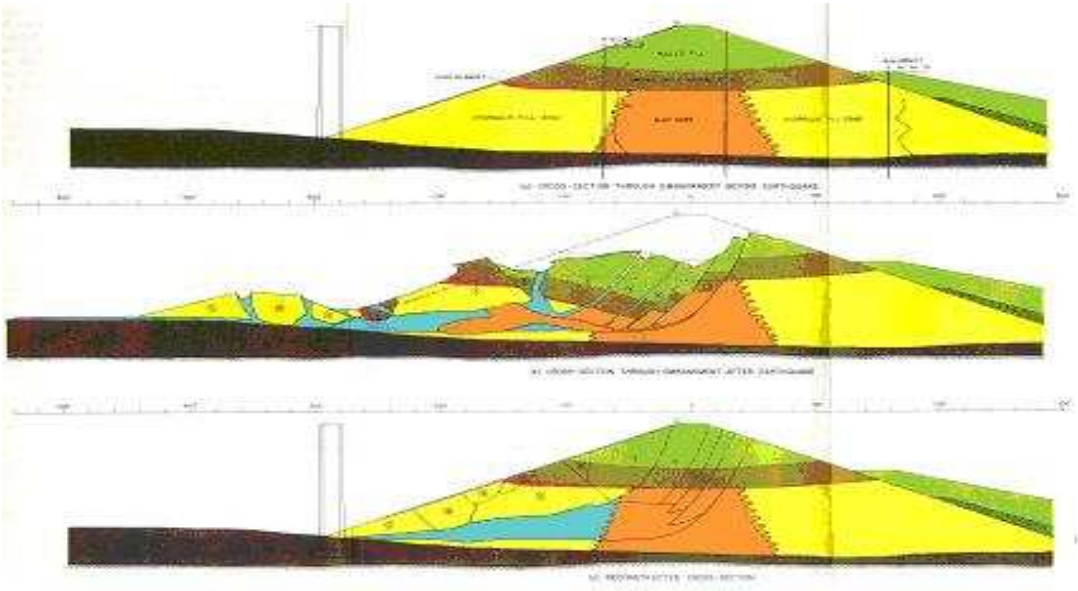

Figure 3: Cross-section of the lower San Fernando Dam through slide area and reconstructed cross section (after Reference [3]).

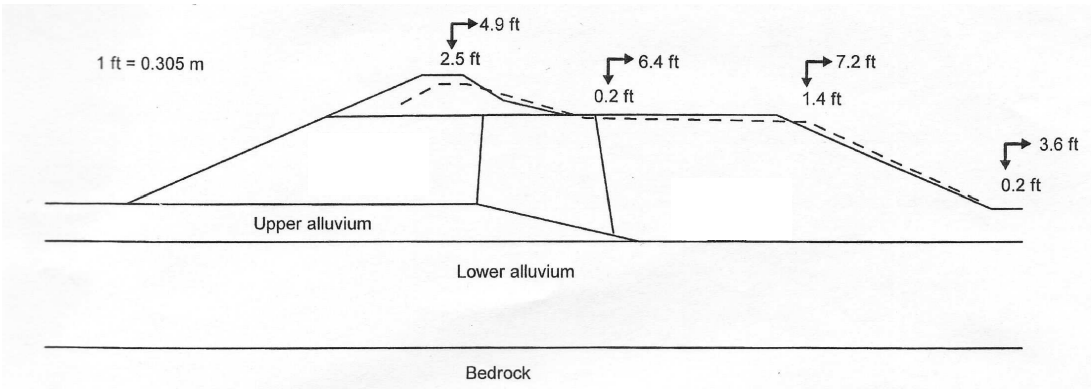

Figure 4: Measured movement at the upper San Fernando Dam (after Reference [4]).

4 Model and Input Motion

Figure 5(a) shows the material zones of the typical cross-section of the Lower San Fernando Dam. The finite element mesh of the typical cross-section are shown in Figure 5(b).

Figure 6(a) shows the material zones of the typical cross-section of the Upper San Fernando Dam. The finite element mesh of the typical cross-section are shown in Figure 6(b).

The modified Pacoima Dam accelerogram with a peak acceleration of 0.6g (Figure 7) as originally used by Seed et al. [1] was used as the input motion at the base of the model.

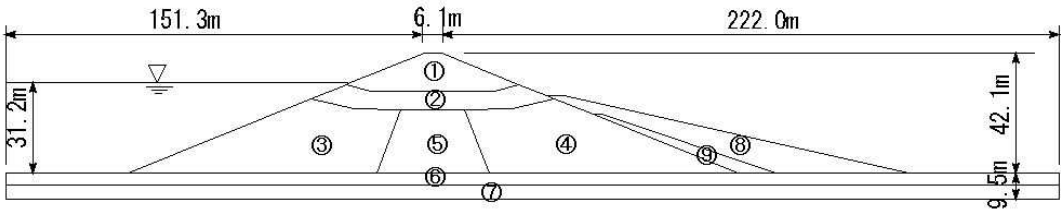

(a) Material zones

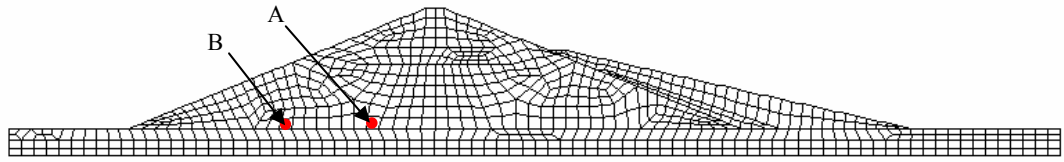

(b) Finite element meshes

Figure 5: Material zones of the Lower San Fernando Dam and finite element meshes.

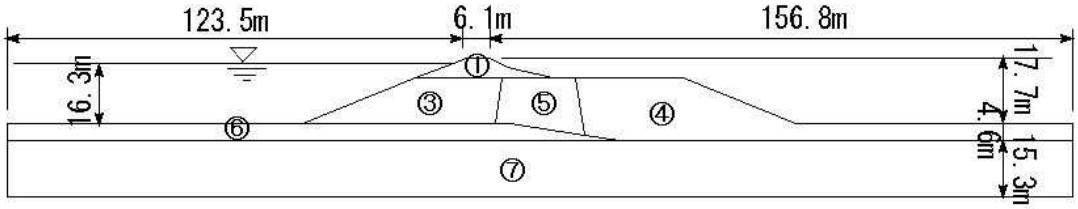

(a) Material zones

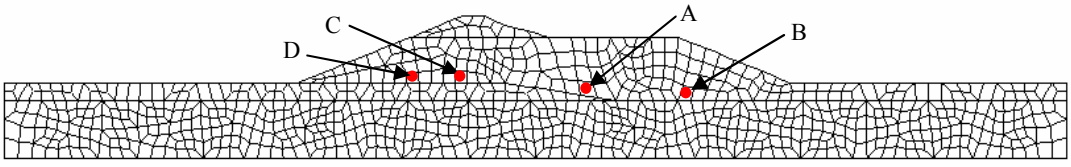

(b) Finite element meshes

Figure 6: Material zones of the Upper San Fernando Dam and finite element meshes.

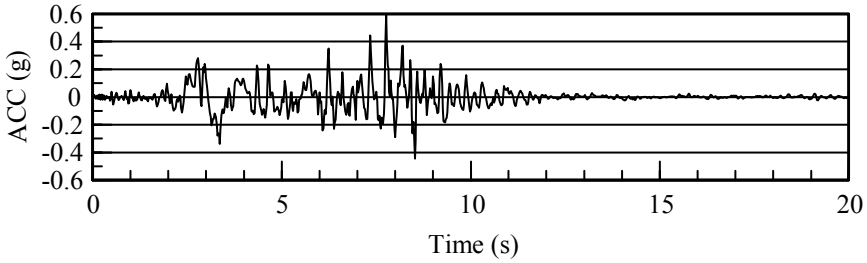

Figure 7: Input motion, modified Pacoima Dam accelerogram.

5 Constitutive Relationship and Parameters

The same number is used for the same material of the Lower and Upper San Fernando Dams in Figure 5(a) and 6(a). The permeability of all kinds of materials used for the steady seepage analysis before the earthquake is listed in Table 1. Table 1 also shows the parameters used to calculate the initial stresses in the embankments before the earthquake and to evaluate the safety factor of the embankment slopes after the excess pore water pressure has induced by the earthquake. Table 2 indicates the parameters of the generalized plasticity model used for the fully coupled dynamic effective-stress analysis. The parameters except M_g and M_f borrowed from Reference [7], and M_g of 1.375 borrowed from Reference [8].

Material number	E (MPa)	ν	c (kPa)	ϕ (°)	γ (kN/m^3)	k_x (10^{-5}m/s)	k_y (10^{-5}m/s)
1	102	0.286	0.0	34	22.0	0.5	0.2
2	102	0.286	0.0	34	22.0	0.5	0.2
3	89	0.286	0.0	34	19.2	10.0	4.0
4	98	0.286	0.0	34	19.2	10.0	4.0
5	153	0.286	0.0	34	19.2	0.5	0.2
6	153	0.286	20.0	37	20.3	1.0	0.4
7	153	0.286	20.0	37	20.3	1.0	0.4
8	102	0.286	0.0	34	22.0	1.0	0.2
9	102	0.286	0.0	34	22.0	1.0	0.2

Table 1: Material properties.

6 Numerical Results of the Lower San Fernando Dam

6.1 Seepage Analysis and Initial Stress Analysis

Figure 8 shows the contours of the pore water pressure in the embankment at the steady state before the earthquake.

Material number	K_0	G_0	M_g	M_f	α_g, α_f	β_0	β_1	H_0	H_{U0} (MPa)	γ, γ_u
1	80	120	1.375	1.032	0.45	4.2	0.2	467.0	40.0	2.0
2	80	120	1.375	1.032	0.45	4.2	0.2	467.0	40.0	2.0
3	70	105	1.375	0.570	0.45	4.2	0.2	408.3	35.0	2.0
4	75	112	1.375	0.825	0.45	4.2	0.2	408.3	37.5	2.0
5	120	180	1.375	1.242	0.45	4.2	0.2	700.0	60.0	2.0
6	120	180	1.375	1.242	0.45	4.2	0.2	700.0	60.0	2.0
7	120	180	1.375	1.242	0.45	4.2	0.2	700.0	60.0	2.0
8	80	120	1.375	1.032	0.45	4.2	0.2	467.0	40.0	2.0
9	80	120	1.375	1.032	0.45	4.2	0.2	467.0	40.0	2.0

Table 2: Parameters of the generalized plasticity model.

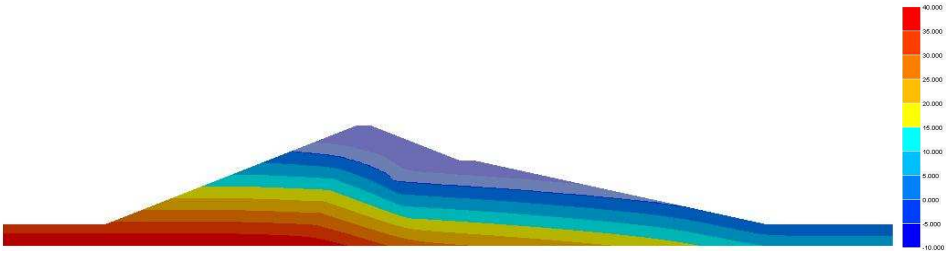

Figure 8: Contours of pore water pressure at steady state for the Lower San Fernando Dam.

6.2 Fully Coupled Dynamic Finite Element Analysis

Figure 9 shows the deformed mesh at 100s after the beginning of the earthquake. The deformation in the upstream shell was so large that we can consider that a failure has occurred. The lateral displacement and its velocity at the toe of the upstream shell are shown in Figure 10. Even after the shaking of the earthquake, the lateral displacement was continually developed with a velocity of about 0.2m/s. During the main shaking to 10s, the times of the maximum velocity of the lateral displacement at the toe of the upstream shell was corresponding to the times of the maximum acceleration of the input motion. After the main shaking, the velocity was significantly reduced from 18s to 25s. Although the velocity changed small from 25s to 100s, the velocity was reduced from 0.24m/s at the time of 35s to 0.14m/s at the time of 55s; however, the velocity was increased to 0.21m/s during 2s at about 55s. This increase in the velocity was considered to be induced by the re-distribution of the excess pore water pressure in the upstream shell. Additionally, the time of the increase in the velocity was consistent with the time of 60s when the failure occurred, reported in Reference [1].

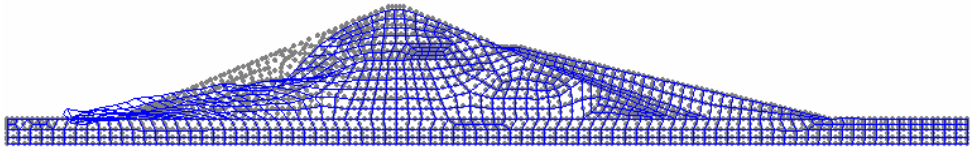

Figure 9: Deformed mesh of the Lower San Fernando Dam at 100s.

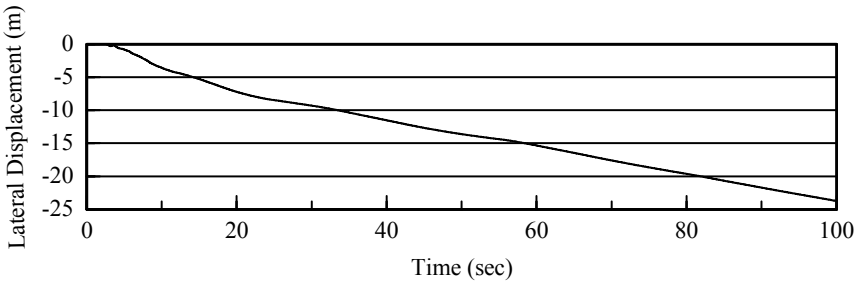

(a) Lateral displacement.

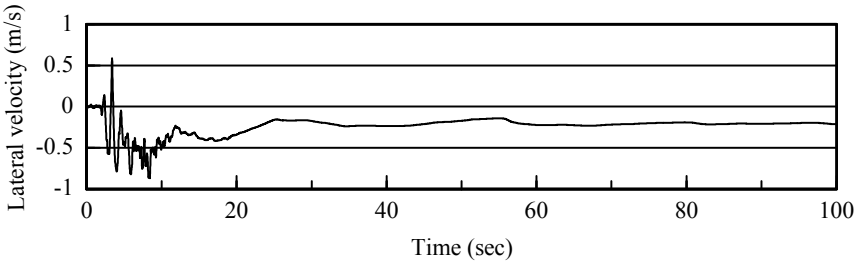

(b) Velocity of lateral displacement.

Figure 10: Time histories of lateral displacement and its velocity at the upstream toe of the Lower San Fernando Dam.

The acceleration responses at representative elevations along the centreline of the cross-section: the crest of the embankment and the top and bottom of the core wall are shown in Figure 11. Compared with the input motion in Figure 7, the high-frequency contents in the input motion were damped out because of the Rayleigh damping and hysteresis damping. The acceleration at the top of the core wall decreased significantly because the soils were loose and liquefied during the earthquake. The acceleration at the crest was amplified again because a dry rolled fill exists at the top of the embankment. The stiffness of the dry rolled fill was not experienced a significant decrease during the earthquake.

Figure 12 shows the distribution of the excess pore water pressure ratio: the ratio of the pore water pressure to the initial vertical effective stress, at 10s and 60s. The excess pore water pressure ratio in the upstream and downstream shell below the phreatic surface was quite high up to about 0.7. This indicate that the hydraulic fill materials in these regions may have either liquefied or been weakened severely. Additionally, the excess pore water pressure ratio in the upstream shell was still high

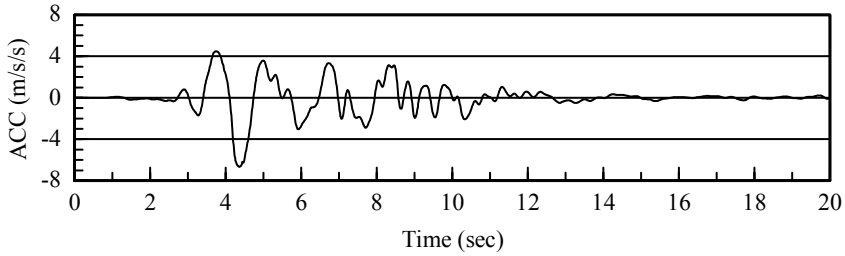

(a) At the crest of the embankment.

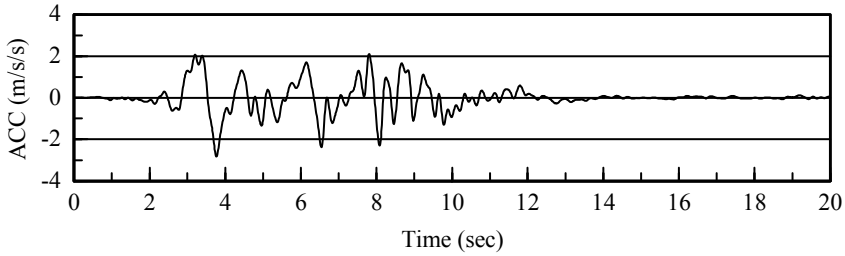

(b) At the top of the core wall.

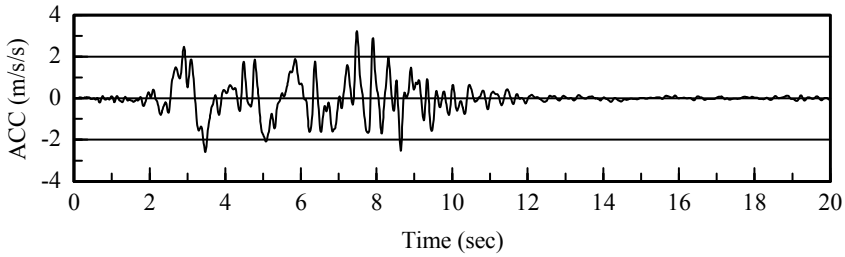

(c) At the bottom of the core wall.

Figure 11: Time histories of acceleration at representative elevations.

even at 60s after the beginning of the earthquake. In the upstream and downstream level ground, the excess pore water pressure was reached unity; however, no significant lateral displacement was calculated because of the absence of a high driving shear stress.

Figures 13 and 14 show the time histories of the excess pore water pressure and excess pore water pressure ratio at two typical points A and B located in the upstream shell. The details of the location of the points A and B can be found Figure 7. Point A locates at the upstream shell and near the core wall; point B locates in the middle of the upstream shell. Both of the two points locate at the bottom of the upstream shell. The excess pore water pressure at point A was about two times of that at point B because the initial vertical effective stress at point A was significantly larger than that at point B. Consequently, the excess pore water pressure ratio at point A was significantly smaller than that at point B. The excess pore water pressure began to dissipate after the main shaking of the earthquake, and the excess pore water pressure of about 100 kPa dissipated from 20s to 100s. In comparison,

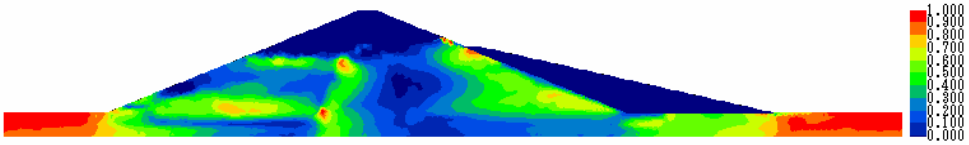

(a) At the time of 10s.

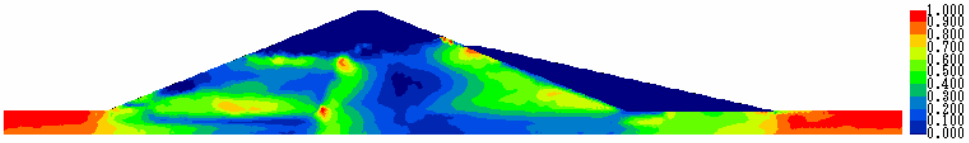

(b) At the time of 60s.

Figure 12: Contours of excess pore water pressure in the Lower San Fernando Dam.

the excess pore water pressure did not decreased until 100s after the beginning of the earthquake. Because the upstream boundary under the water level was assumed to be drained in the fully coupled dynamic effective-stress analysis, the water during the dissipation of the excess pore water pressure in the upstream shell was flowed to upstream. Because the excess pore water pressure at point A was 150 kPa larger than that at point B, the dissipation of the excess pore water at point B was cancelled out by the increase of the excess pore water pressure due to the higher excess pore water pressure in the zone at the right of point B. Consequently, the excess pore water pressure at point B did not decrease after the main shaking of the earthquake within

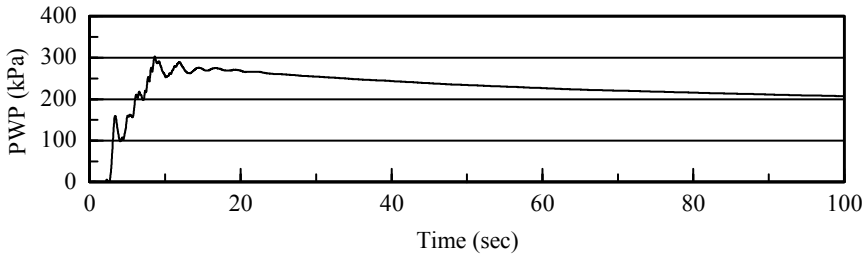

(a) Excess pore water pressure.

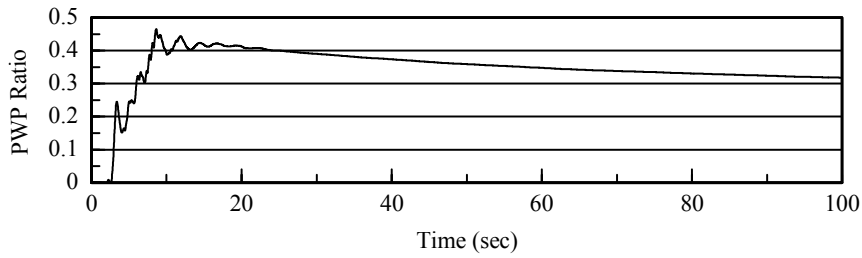

(b) Excess pore water pressure ratio.

Figure 13: Time histories of excess pore water pressure and excess pore water pressure ratio at point A.

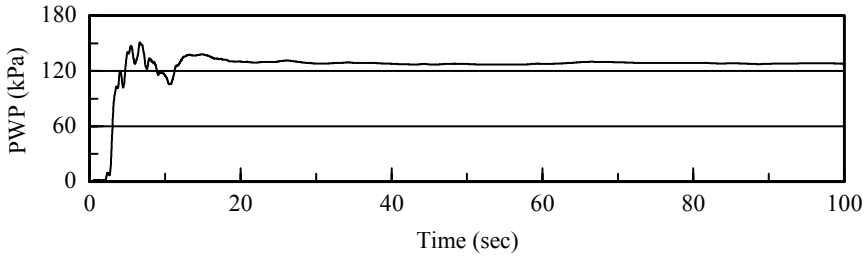

(a) Excess pore water pressure.

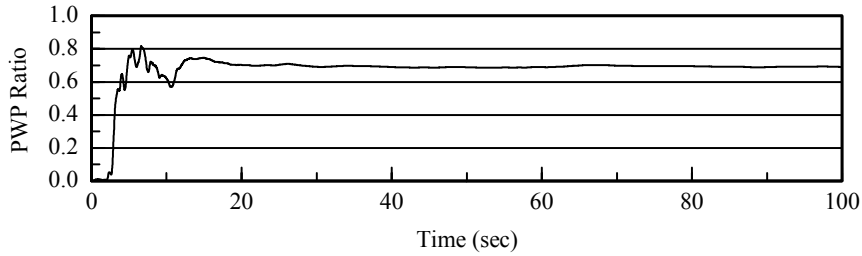

(b) Excess pore water pressure ratio.

Figure 14: Time histories of excess pore water pressure and excess pore water pressure ratio at point B.

the calculation duration of 100s. Moreover, the excess pore water pressure at point B increased about 2.5 kPa at the time of about 60s when the main slide occurred in the upstream shell.

7 Numerical Results of the Upper San Fernando Dam

7.1 Seepage Analysis and Initial Stress Analysis

Figure 15 shows the contours of the pore water pressure in the embankment at the steady state before the earthquake.

7.2 Fully Coupled Dynamic Finite Element Analysis

Figure 16 shows the deformed mesh at 100s for the Upper San Fernando Dam after the beginning of the earthquake. The deformation in the upstream shell of the Upper San Fernando Dam was significantly smaller than that of the Lower San Fernando Dam. Figure 17 shows the time histories of the lateral displacement at the downstream berm and at the downstream toe. The lateral displacement stopped with the finish of the main shaking of the earthquake. The calculated lateral displacements were 2.5m at the downstream berm and 1.2m at the downstream toe; they were consistent with the observation of 2.2m at the downstream berm and 1.1m at the downstream toe.

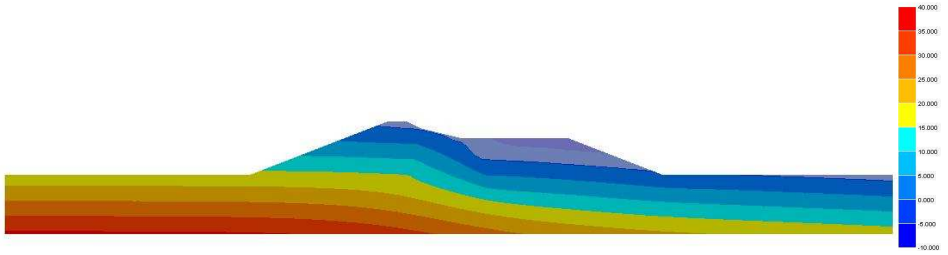

Figure 15: Contours of pore water pressure at steady state for the Upper San Fernando Dam.

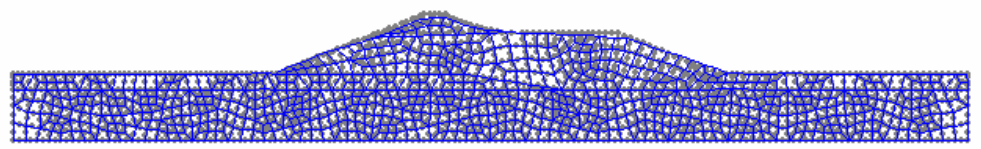

Figure 16: Deformed mesh of the Upper San Fernando Dam at 100s.

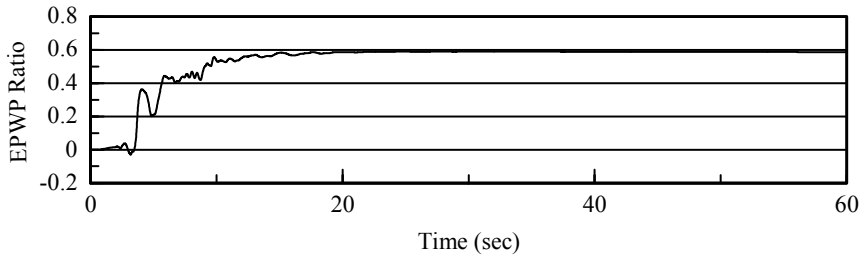

(a) At the downstream berm.

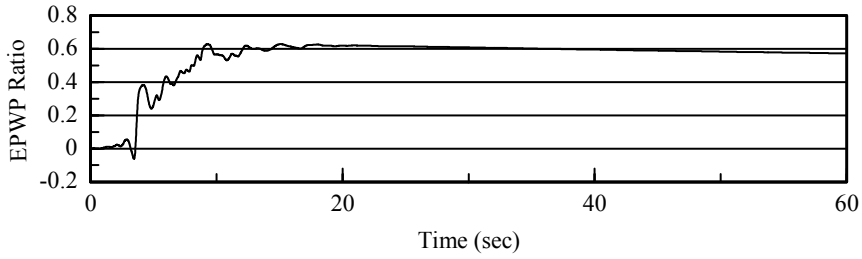

(b) At the downstream toe.

Figure 17: Time histories of lateral displacement at representative points of the Upper San Fernando Dam.

Figure 18 shows the distribution of the excess pore water pressure ratio in the Upper San Fernando Dam at 10s and 60s. The excess pore water pressure ratio in the upstream shell of the Upper San Fernando Dam is about 0.6, and the excess pore

water pressure ratio kept still high 60s after the beginning of the earthquake. The excess pore water pressure ratio in the Upper San Fernando Dam is about 0.1 lower than that in the Lower San Fernando Dam. Because the Lower San Fernando Dam is 25m higher than the Upper San Fernando Dam, the shear stress before the earthquake in the Lower San Fernando Dam is larger than that in the Upper San Fernando Dam. This is the one of the main reason that a large slide occurred in the upstream of the Lower San Fernando Dam but only some residual displacement occurred in the Upper San Fernando Dam.

Figure 19 shows the time histories of the excess pore water pressure ratio at representative points A and B in the downstream shell and points C and D in the upstream shell of the Upper San Fernando Dam.

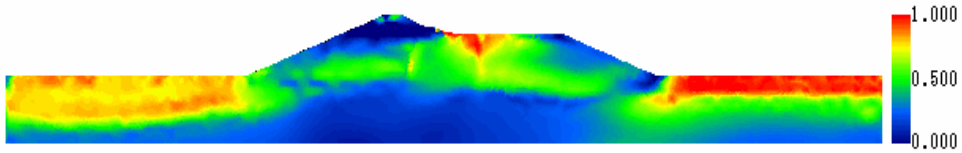

(a) At the time of 10s.

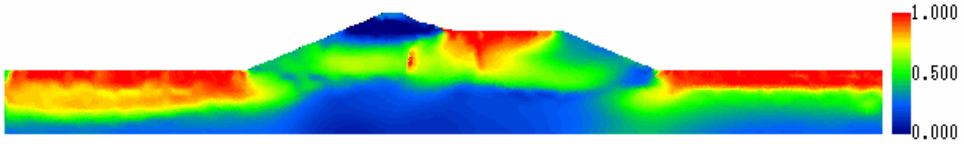

(b) At the time of 60s.

Figure 18: Contours of excess pore water pressure in the Upper San Fernando Dam.

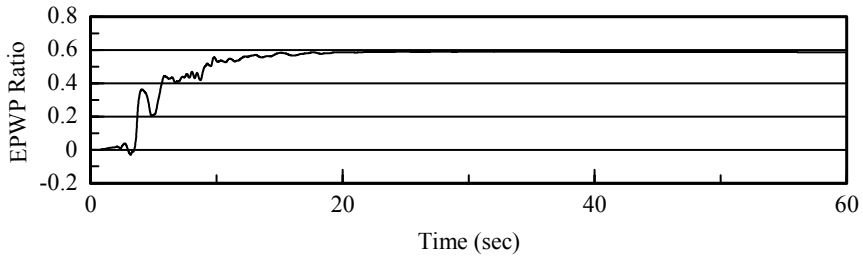

(a) At point A in the downstream shell.

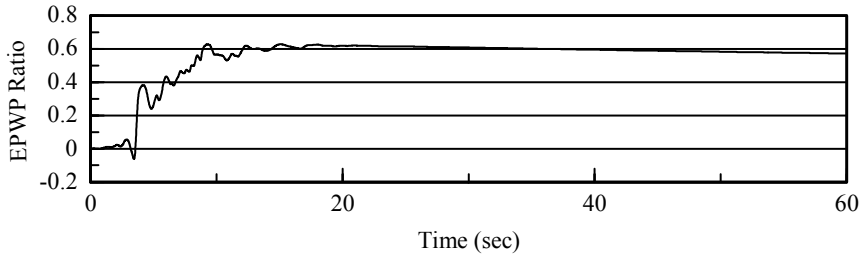

(b) At point B in the downstream shell.

(Continued to the next page)

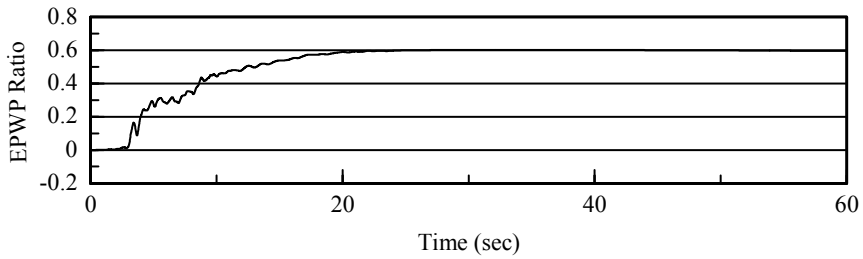

(c) At point C in the upstream shell.

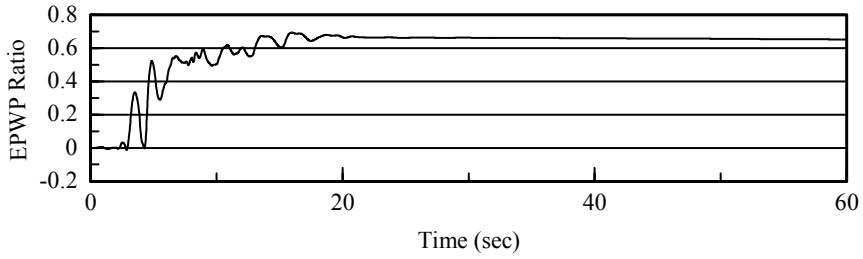

(d) At point D in the upstream shell.

Figure 19: Time histories of excess pore water pressure ratio at representative points in the Upper San Fernando Dam.

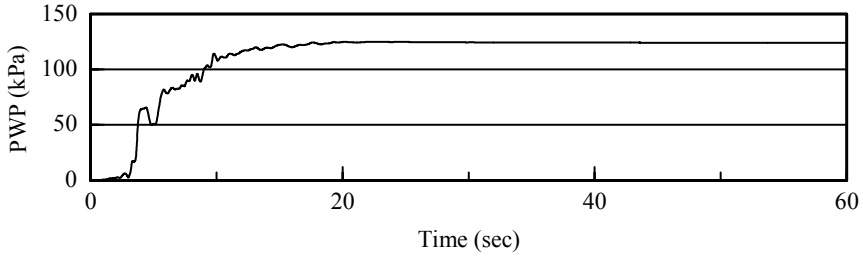

(a) At point A in the downstream shell.

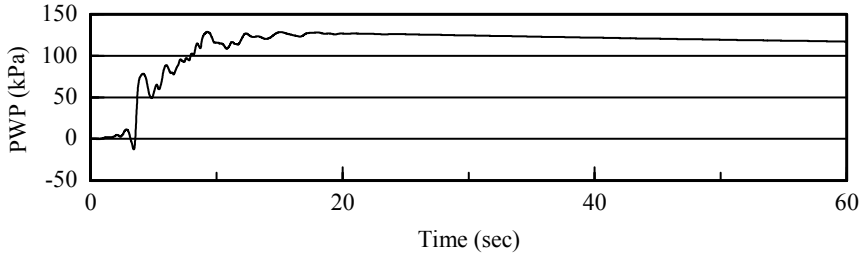

(b) At point B in the downstream shell.

Figure 20: Time histories of excess pore water pressure at points A and B in the downstream shell of the Upper San Fernando Dam.

Figure 20 shows the time histories of the excess pore water pressure at points A and B in the downstream shell of the Upper San Fernando Dam. The initial vertical effective stresses at the two points are almost the same as one another, and the excess pore water pressure at the two points was also almost identical to one another. The excess pore water pressure at point A almost did not dissipate during 40s after the main shaking of the earthquake. In comparison, the excess pore water pressure at point B dissipated slightly because point B is nearer the drained downstream boundary. The significant re-distribution of the excess pore water pressure happened in the upstream shell of the Lower San Fernando Dam did not occur in the downstream shell of the Upper San Fernando Dam.

8 Stability Analyses

The seismic coefficient method and Δu-method were used the safety factor of the Lower and Upper San Fernando Dams. Here, the simplified Bishop's method was used to calculate the safety factor. In the seismic coefficient method, the horizontal seismic coefficient was assumed to 0.15, and the consolidated undrained shear strength: c=57.5kPa, ϕ=20º for materials 1-5 and 8 and 9, c=74.4kPa, ϕ=27º for materials 6 and 7. The calculated factor of safety of the upstream shell of the Lower San Fernando Dam was 1.156, which was consistent with 1.20 reported by Seed et al. [1]. Obviously, the seismic coefficient method can not explain the major slide occurred in the upstream shell of the Lower San Fernando Dam. The factors of safety of the upstream and downstream shells of the Upper San Fernando Dam were 2.163 and 2.005 respectively. In the Δu-method in this paper, the pore water pressure in the steady state condition and the excess pore water pressure were summed up and used to calculate the safety factor. The calculated factor of safety of the upstream shell of the Lower San Fernando Dam was 1.356. The factors of safety of the upstream and downstream shells of the Upper San Fernando Dam were 1.253 and 1.164 respectively.

The finite element method in conjunction with the shear reduction technique was also used to calculate the factor of safety. The consideration of the pore water pressure was the same as that in the Δu-method. The calculated factor of safety of the upstream shell of the Lower San Fernando Dam was 0.88. This can explain why the major slide occurred in the upstream shell of the Lower San Fernando Dam during the 1971 San Fernando Earthquake. And the sliding surface can be estimated using the incremental shear strain at the last step of the incremental calculation of the finite element analysis. Figure 21 shows that, for the Lower San Fernando Dam,

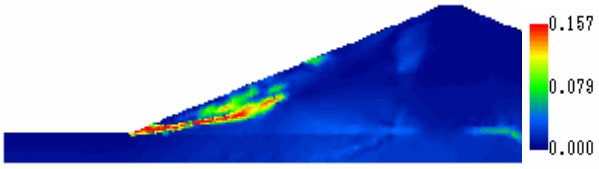

Figure 21: Incremental shear strain at the last step of the finite element method in conjunction with shear strength reduction technique.

the siding surface first occurred near the toe of the upstream. This was consistent with the failure mechanism observed, as shown in Figure 3.

9 Conclusions

Seismic safety evaluation procedure currently used in Japan first calculates the factor of safety using Δu-method, in which the excess pore water pressure is simply evaluated based on the simple liquefaction evaluation, or seismic coefficient method assuming a circular slip surface. If the calculated factor of safety is smaller than the planned one, dynamic analysis has to be conducted to calculate the residual displacement under strong earthquake. However, because the slip surface is most possibly non-circular for liquefiable embankments, and because the seismic characteristics are not considered for Δu-method or seismic coefficient method, the residual displacement cannot be calculated with a satisfactorily confidence. This paper proposes to use finite element approaches to evaluate the seismic safety of embankments under strong earthquake; in details, we use seepage analysis to calculate the pore water pressure before earthquake, use fully coupled dynamic elastoplastic finite element approach to calculate the deformation and excess pore water pressure induced by strong earthquake, and use static elastoplastic finite element method with shear strength reduction technique to evaluate the safety of embankments after strong earthquake considering the pore water pressure and excess pore water pressure calculated by finite element seepage analysis and fully coupled dynamic elastoplastic finite element approach. The factor of safety of embankments of finite element approaches is compared with those of conventional Δu-method or seismic coefficient method.

The proposed approaches are used to re-analyze the famous Lower and Upper San Fernando Dams. During the San Fernando earthquake of February 9, 1971 (magnitude 6.6), a major slide occurred in the upstream slope of the Lower San Fernando Dam; slide movements also caused a downstream movement of about 1.5m in the embankment of the Upper San Fernando Dam; however, a major slide did not occur. For the Lower San Fernando Dam, numerical results can re-produce the major slide with a large residual displacement and a factor of safety after the earthquake is 0.88 when the excess pore water pressure due to the liquefaction was considered. For the Upper San Fernando Dam, the calculated residual displacement after the earthquake was consistent with the observations, and the factor of safety for the downstream shell is larger than one even the excess pore water pressure was considered.

References

[1] H.B. Seed, I.M. Idriss, K.L. Lee, F.I. Makdisi, “Dynamic analysis of the slide in the Lower San Fernando Dam during the earthquake of February 9, 1971”, Journal of the Geotechnical Engineering Division, ASCE, 101(9), 889-911, 1975.

[2] H.B. Seed, “The Rankine lecture: Considerations in the earthquake-resistant design of earth and rockfill dams”, Geotechnique, 29(1), 215-263, 1979.
[3] H.B. Seed, K.L. Lee, I.M. Idriss, F.I. Makdisi, “The slides in the San Fernando Dams during the earthquake of February 9, 1971”, Journal of the Geotechnical Engineering Division, ASCE, 101(7), 651-688, 1975.
[4] G. Wu, “Earthquake-induced deformation analyses of the upper San Fernando Dam under the 1971 San Fernando Earthquake”, Canadian Geotechnical Journal, 38, 1-15, 2001.
[5] M.M. Farias, D.J. Naylor, “Safety analysis using finite element”, Computers and Geotechnics, 22(2), 165-181, 1998.
[6] M. Pastor, O.C. Zienkiewicz, A.H.C. Chan, “Generalized plasticity and the modelling of soil behaviour”, International Journal for Numerical and Analytical Methods in Geomechanics, 14, 151-190, 1990.
[7] O.C. Zienkiewicz, A.H.C. Chan, M. Pastor, B.A. Schrefler, T. Shiomi, “Computational Geomechanics with a Special Reference to Earthquake Engineering”, John Wiley & Sons Ltd., Chichester, 1999.
[8] H.Y. Ming, X.S. Li, “Fully coupled analysis of failure and remediation of Lower San Fernando Dam”, Journal of Geotechnical and Geoenvironmental Engineering, 129(4), 336-349, 2003.
[9] Forum 8 Co., Ltd., “User’s manual of VisualFEA+VGFlow”, 2004 (in Japanese).
[10] Forum 8 Co., Ltd., “User’s manual of UWLC”, 2004 (in Japanese).
[11] Forum 8 Co., Ltd., “User’s manual of GeoFEAS”, 2005 (in Japanese).
[12] D.V. Griffiths, P.A. Lane, “Slope stability analysis by finite elements”, Geotechnique, 49(3), 387-403, 1999.